

# Cold interactions between an $\text{Yb}^+$ ion and a Li atom: Prospects for sympathetic cooling, radiative association, and Feshbach resonances

Michał Tomza,<sup>1,2</sup> Christiane P. Koch,<sup>2</sup> and Robert Moszynski<sup>1</sup>

<sup>1</sup>*Faculty of Chemistry, University of Warsaw, Pasteura 1, 02-093 Warsaw, Poland*

<sup>2</sup>*Theoretische Physik, Universität Kassel, Heinrich-Plett-Strasse 40, 34132 Kassel, Germany*

(Received 3 September 2014; revised manuscript received 14 January 2015; published 17 April 2015)

The electronic structure of the  $(\text{LiYb})^+$  molecular ion is investigated with two variants of the coupled cluster method restricted to single, double, and noniterative or linear triple excitations. Potential-energy curves for the ground and excited states, permanent and transition electric dipole moments, and long-range interaction coefficients  $C_4$  and  $C_6$  are reported. The data are subsequently employed in scattering calculations and photoassociation studies. Feshbach resonances are shown to be measurable, despite the ion's micromotion in the Paul trap. Molecular ions can be formed in their singlet electronic ground state by one-photon photoassociation and in triplet states by two-photon photoassociation; and control of cold atom-ion chemistry based on Feshbach resonances should be feasible. Conditions for sympathetic cooling of an  $\text{Yb}^+$  ion by an ultracold gas of Li atoms are found to be favorable in the temperature range 10 nK–10 mK, and further improvements using Feshbach resonances should be possible. Overall, these results suggest excellent prospects for building a quantum simulator with ultracold  $\text{Yb}^+$  ions and Li atoms.

DOI: [10.1103/PhysRevA.91.042706](https://doi.org/10.1103/PhysRevA.91.042706)

PACS number(s): 34.70.+e, 34.50.Cx, 33.80.-b, 34.20.-b

## I. INTRODUCTION

Trapped ions are a highly controllable system with strong interactions and thus find many applications, for example in precision measurements, quantum computing, or quantum sensing [1–3]. Currently, a growing number of experiments combine trapped ions with ultracold atoms [4–15], allowing one to study the dynamics of a single ion immersed in an atomic Bose-Einstein condensate [4] or to control chemical reactions of a single ion and ultracold atoms [6]. Further prospects include the idea to build a quantum simulator with a hybrid system of ultracold ions and atoms to emulate solid-state physics [16,17] or to form ultracold molecular ions [18].

Any experimental proposal based on a hybrid system of ultracold ions and atoms has to face two issues. The first one is the choice of trapping method for the ions; the second one is potential losses due to chemical reactions between ions and atoms. Although optical traps for ions have become available [19,20], radio-frequency (rf) based Paul traps still constitute the most popular choice [21]. Unfortunately, the time-dependent rf potential induces micromotion of the ion that limits the minimum temperature that can be achieved [22–24].

The impact of micromotion can be minimized by choosing a large ion to atom mass ratio [22]. An  $\text{Yb}^+$  ion immersed in an ultracold gas of Li atoms is thus a perfect candidate to construct a hybrid ion-atom experiment. Besides the large ion to atom mass ratio to facilitate cooling, the relatively simple electronic structure of the  $(\text{LiYb})^+$  molecular ion, with the entrance channel  $\text{Yb}^+(^2S)+\text{Li}(^2S)$  well separated from other electronic states, reduces potential nonradiative losses. Nevertheless, to estimate the rates for radiative loss as well as the ratio of elastic to inelastic collision cross sections, reliable knowledge of the electronic structure is needed. This is essential both for realizing sympathetic cooling of the ion by the atoms [4,5] and for the coupling a crystal of trapped  $\text{Yb}^+$  ions to a cloud of ultracold fermionic Li atoms, as proposed for building a quantum simulator to emulate solid-state physics

[17]. All relevant processes are schematically summarized in Fig. 1.

Here we theoretically investigate the electronic structure and collisional properties of the  $\text{Yb}^+$  ion interacting with the Li atom [25]. We report an *ab initio* study of the interactions of the  $\text{Yb}^+$  ion with the Li atom, the system of interest in an ongoing experiment [26]. First, we investigate the electronic structure of the  $(\text{LiYb})^+$  molecular ion by means of state-of-the-art *ab initio* techniques. Next, we employ the electronic structure data to investigate the prospects for sympathetic cooling, spontaneous radiative association, laser-induced association (photoassociation), and observation of Feshbach resonances. Special attention is paid to the formation of molecular ions by means of both spontaneous radiative association as well as stimulated photoassociation and to the control of chemical reactivity with both laser and magnetic fields.

The plan of our paper is as follows. Section II describes the theoretical methods used in the electronic structure and scattering calculations. Section III presents the results of the *ab initio* calculations in Sec. III A, followed by a discussion of elastic collisions, radiative charge transfer, radiative association, and Feshbach resonances in Secs. III B–III F. A critical assessment of our findings in view of their implication for experiment, in particular in terms of the prospects for sympathetic cooling, is provided in Sec. III D. Section IV summarizes our paper.

## II. COMPUTATIONAL DETAILS

### A. Electronic structure calculations

We adopt the computational scheme successfully applied to the ground and excited states of the  $\text{SrYb}$  [27] and  $\text{Sr}_2$  [28] molecules as well as the  $(\text{BaRb})^+$  molecular ion [29]. The potential-energy curve for the  $X^1\Sigma^+$  ground electronic state is obtained with the coupled cluster method restricted to single, double, and noniterative triple excitations [CCSD(T)] [30]. Potential-energy curves for the lowest states in the  $^3\Sigma$  and  $^3\Pi$  symmetries are obtained with the spin-restricted open-shell

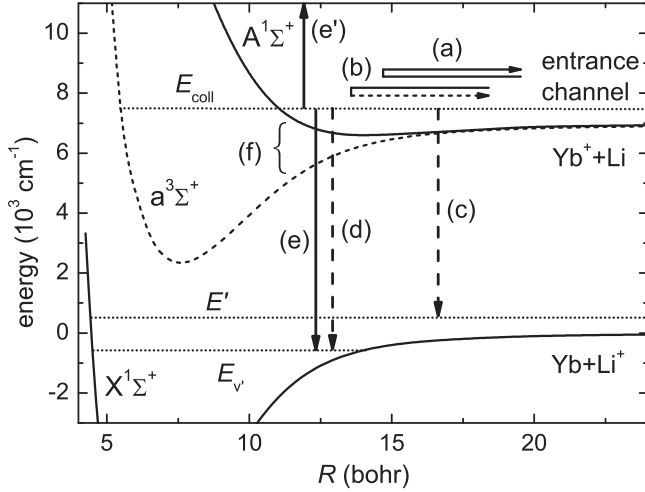


FIG. 1. Interaction between an  $\text{Yb}^+$  ion and a Li atom. The collision can entail the following processes: elastic scattering (a), superelastic (spin-changing) scattering (b), radiative charge transfer (c), radiative association (d), photoassociation to ground (e) or excited (e') states, and Feshbach resonance based magnetoassociation (f).

coupled cluster method restricted to single, double, and noniterative triple excitations [RCCSD(T)] [31]. Calculations of all other excited states employ the linear-response theory (equation of motion) within the coupled cluster singles, doubles, and linear triples framework (LRCC3) [32,33]. The basis set superposition error is corrected by using the counterpoise correction of Boys and Bernardi [34]. The CCSD(T) and RCCSD(T) calculations were performed with the MOLPRO suite of codes [35], while LRCC3 calculations were carried out with the DALTON program [36].

The lithium atom is described by the augmented core-valence correlation consistent polarized valence quadruple- $\zeta$  quality basis set, aug-cc-pCVQZ. For the ytterbium atom, the scalar relativistic effects are accounted for by using the small-core fully relativistic energy-consistent pseudopotential ECP28MDF [37] to replace the inner-shell electrons, and the associated basis set  $(15s\ 14p\ 12d\ 11f\ 8g)/[8s\ 8p\ 7d\ 7f\ 5g]$  is employed. Due to the less efficient numerical code for the LRCC3 method it was computationally not feasible to carry out calculations for excited states correlating all electrons included in the model and using the large basis set. Therefore in these calculations, the core electrons are frozen and only the 12 outer-shell electrons are correlated. The small-core energy consistent pseudopotential was used also in these calculations, instead of an existing large-core one, to avoid potentially different systematic errors for different potential-energy curves.

The long-range asymptotics of the potentials is computed from Eqs. (4)–(8) of Ref. [29]. The dynamic polarizability at imaginary frequency of the  $\text{Yb}^+$  ion and the Li atom are obtained by using the explicitly connected representation of the expectation value and polarization propagator within the coupled cluster method [38,39] and the best approximation within the coupled cluster method XCCSD4 [40]. The dynamic polarizability at imaginary frequency of the Li atom is taken from Ref. [41] and the dynamic polarizability of the  $\text{Yb}^+$

ion is obtained from the sum over state expression using the transition moments [42]. The static quadrupole polarizabilities of the Li and Yb atoms are taken from accurate atomic calculations reported in Refs. [43] and [44], respectively.

## B. Scattering calculations

In this subsection, we provide a brief summary of all equations employed in our scattering calculations [45–54].

The Hamiltonian describing the nuclear motion of the  $(\text{LiYb})^+$  molecular ion reads

$$\hat{H} = -\frac{\hbar^2}{2\mu} \frac{1}{R} \frac{d^2}{dR^2} R + \frac{\hat{l}^2}{2\mu R^2} + \sum_{S, M_S} V_S(R) |S, M_S\rangle \langle S, M_S| + V^{ss}(R) + V^{so}(R) + \hat{H}_{\text{Yb}^+} + \hat{H}_{\text{Li}}, \quad (1)$$

where  $R$  denotes the internuclear distance,  $\hat{l}$  is the rotational angular momentum operator,  $\mu$  is the reduced mass, and  $V_S(R)$  is the potential-energy curve for the state with total electronic spin  $S$ . The relativistic terms  $V^{ss}(R)$  and  $V^{so}(R)$  stand for, respectively, the spin-dipole-spin-dipole interaction responsible for the dipolar relaxation [45] and the second-order spin-orbit term [46]. The atomic Hamiltonian,  $\hat{H}_j$  ( $j = \text{Yb}^+, \text{Li}$ ), including Zeeman and hyperfine interactions, is given by

$$\hat{H}_j = \zeta_j \hat{i}_j \cdot \hat{s}_j + (g_e \mu_B \hat{s}_{j,z} + g_j \mu_N \hat{i}_{j,z}) B_z \quad (2)$$

with  $\hat{s}_j$  and  $\hat{i}_j$  the electron- and nuclear-spin operators,  $\zeta_j$  denoting the hyperfine coupling constant,  $g_{e/j}$  the electron and nuclear  $g$  factors, and  $\mu_{B/N}$  the Bohr and nuclear magnetons. For a fermionic  $\text{Yb}^+$  ion, Eq. (2) reduces to the electronic Zeeman term. We neglect the unknown second-order spin-orbit coupling  $V^{so}(R)$  which has the same form and a similar effect as the spin-spin coupling  $V^{ss}(R)$  [45,46].

The bound rovibrational levels are calculated by diagonalizing the nuclear Hamiltonian represented on a Fourier grid with adaptive step size [47–49]. The total scattering wave function is constructed in a fully uncoupled basis set,

$$|i_{\text{Yb}^+}, m_i, \text{Yb}^+\rangle |s_{\text{Yb}^+}, m_s, \text{Yb}^+\rangle |i_{\text{Li}}, m_i, \text{Li}\rangle |s_{\text{Li}}, m_s, \text{Li}\rangle |l, m_l\rangle,$$

with  $m_j$  the projection of angular momentum  $j$  on the space-fixed  $Z$  axis, assuming the projection of the total angular momentum  $M_{\text{tot}} = m_{f, \text{Yb}^+} + m_{f, \text{Li}} + m_l = m_{i, \text{Yb}^+} + m_{s, \text{Yb}^+} + m_{i, \text{Li}} + m_{s, \text{Li}} + m_l$ , to be conserved. The coupled channel equations are solved using a renormalized Numerov propagator [55] with step-size doubling and about 100 step points per de Broglie wavelength. The wave function ratio  $\Psi_{i+1}/\Psi_i$  at the  $i$ th grid step is propagated to large interatomic separations, transformed to the diagonal basis, and the  $K$  and  $S$  matrices are extracted by imposing long-range scattering boundary conditions in terms of Bessel functions.

The rate constant for elastic collisions in the  $i$ th channel is given by the diagonal elements of the  $S$  matrix summed over partial waves  $l$ ,

$$K_{\text{el}}^i(E) = \frac{\pi \hbar}{\mu k} \sum_{l=0}^{\infty} (2l+1) |1 - S_{ii}^l(E)|^2, \quad (3)$$

where  $k = \sqrt{2\mu E/\hbar^2}$  with collision energy  $E$ . Similarly, the scattering length is obtained from the  $S$  matrix (for  $l = 0$ ),

$$a = \frac{1}{ik} \frac{1 - S_{11}}{1 + S_{11}}. \quad (4)$$

Spontaneous radiative processes are governed by the Einstein coefficients. For transitions between two bound rovibrational states  $vl$  and  $v'l'$ , between a scattering state of energy  $E$  and a bound state  $v'l'$ , and between two scattering states of energies  $E$  and  $E'$ , they are given by

$$A_{vl,v'l'} = \frac{4\alpha^3}{3e^4\hbar^2} H_l (E_{vl} - E_{v'l'})^3 |\langle \Psi_{vl} | d(R) | \Psi_{v'l'} \rangle|^2, \quad (5a)$$

$$A_{El,v'l'} = \frac{4\alpha^3}{3e^4\hbar^2} H_l (E - E_{v'l'})^3 |\langle \Psi_{El} | d(R) | \Psi_{v'l'} \rangle|^2, \quad (5b)$$

$$A_{El,E'l'} = \frac{4\alpha^3}{3e^4\hbar^2} H_l (E - E')^3 |\langle \Psi_{El} | d(R) | \Psi_{E'l'} \rangle|^2, \quad (5c)$$

respectively. In Eq. (5) the primed and unprimed quantities pertain to the ground- and excited-state potentials, respectively,  $d(R)$  is the transition dipole moment from the ground to the excited electronic state,  $\alpha$  is the fine-structure constant, and  $e$  is the electron charge. The Hönl-London factor  $H_l$  is equal to  $(l+1)/(2l+1)$  for the  $P$  branch ( $l = l' - 1$ ), and to  $l/(2l+1)$  for the  $R$  branch ( $l = l' + 1$ ). In Eq. (5), the scattering states  $|\Psi_{El}\rangle$  are energy normalized, whereas the wave functions of bound levels are normalized to unity, such that the three types of Einstein coefficients have different dimensions.

Radiative charge transfer can be described by the following Fermi “golden rule” type expression for the rate constant [50–52],

$$K_{\text{CT}}(E) = \frac{4\pi^2\hbar^2}{\mu k} \sum_{l=0}^{\infty} (2l+1) \sum_{l'=l\pm 1} \int_0^{\infty} A_{El,E'l'} d\varepsilon, \quad (6)$$

where  $\varepsilon = E - E'$ . Analogously, the rate constant for radiative association is given by

$$K_{\text{RA}}(E) = \frac{4\pi^2\hbar^2}{\mu k} \sum_{l=0}^{\infty} (2l+1) \sum_{l'=l\pm 1} \sum_{v'} A_{El,v'l'}. \quad (7)$$

The total rate constant for radiative losses is the sum of Eqs. (6) and (7),

$$K_{\text{R}}(E) = K_{\text{CR}}(E) + K_{\text{RA}}(E). \quad (8)$$

Stimulated radiative association (photoassociation) becomes possible by applying a laser field. The rate constant for photoassociation reads [56,57]

$$K_{\text{PA}}(\omega, E) = \frac{\pi\hbar}{\mu k} \sum_{l=0}^{\infty} (2l+1) \sum_{v'l'} |S_{v'l'}(E, l, \omega)|^2, \quad (9)$$

with

$$|S_{v'l'}(E, l, \omega)|^2 = \frac{\gamma_{v'l'}^s(E, l) \gamma_{v'l'}^d}{[E - \Delta_{v'l'}(\omega)]^2 + \frac{1}{4} [\gamma_{v'l'}^s(E, l) + \gamma_{v'l'}^d]^2}, \quad (10)$$

where  $\gamma_{v'l'}^s(E, l)$  is the stimulated emission rate, and  $\gamma_{v'l'}^d$  is the rate for spontaneous decay.  $\Delta_{v'l'}(\omega)$  is the detuning relative to the position of the bound rovibrational level  $v'l'$ , i.e.,  $\Delta_{v'l'} =$

$E_{v'l'} - \hbar\omega$  with  $E_{v'l'}$  the binding energy of level  $v'l'$ . The spontaneous emission rates  $\gamma_{v'l'}^d$  are obtained from the Einstein coefficients  $A_{v'l',vl}$ ,

$$\gamma_{v'l'}^d = \sum_{vl} A_{v'l',vl} + \sum_l \int_0^{\infty} A_{v'l',El} d\varepsilon. \quad (11)$$

At low laser intensity  $I$ , the stimulated emission rate is given by the Fermi golden rule expression

$$\gamma_{v'l'}^s(E, l) = 4\pi^2 \frac{I}{\epsilon_0 c} (2l'+1) H_{l'} |\langle \Psi_{El} | d(R) | \Psi_{v'l'} \rangle|^2. \quad (12)$$

Equations (6), (7), and (9) give rate constants for a single scattering energy  $E$ . In practice, we have an ensemble of thermally populated states and the rate constants at a temperature  $T$  are obtained by performing a Boltzmann average,

$$K(T) = \frac{2}{\sqrt{\pi} (k_B T)^{3/2}} \int_0^{\infty} K(E) \sqrt{E} e^{-E/k_B T} dE. \quad (13)$$

Hereafter, when we speak about the rate constant for a given collision energy we mean  $K(E)$ , whereas the rate constant for a given temperature implies  $K(T)$ .

### III. NUMERICAL RESULTS AND DISCUSSION

#### A. Potential-energy curves, permanent and transition electric dipole moments

Before presenting our potential-energy curves, and permanent and transition dipole moments, we first compare the computed atomic results to the best available experimental data. Our predicted position of the nonrelativistic  $^2P$  state of the Li atom is  $14910 \text{ cm}^{-1}$ , to be compared with the experimental value of  $14904 \text{ cm}^{-1}$  [58]. For the  $^3P$  state of the Yb atom we obtain  $17635 \text{ cm}^{-1}$ , in a relatively good agreement with the experimental value of  $18903 \text{ cm}^{-1}$  [58]. The predicted ionization potentials (IPs) are  $43464 \text{ cm}^{-1}$  for Li and  $50267 \text{ cm}^{-1}$  for Yb, in good agreement with the experimental values of  $43487 \text{ cm}^{-1}$  and  $50443 \text{ cm}^{-1}$  [58], respectively. To further assess the quality of the methods, basis sets, and pseudopotential employed in the present work, we have computed the static polarizabilities of the ground state of the Li and Yb atoms and of the ground state of the Li<sup>+</sup> and Yb<sup>+</sup> ions. Our calculated polarizability of the Li atom ground state amounts to  $164.3a_0^3$ . The experimental value is  $164.0 \pm 3.4a_0^3$  [59], while the best theoretical result is  $164.0a_0^3$  [41]. Also the static polarizability of the Li<sup>+</sup> ion,  $0.190a_0^3$ , is in very good agreement with the experimental value of  $0.188 \pm 0.002a_0^3$  [60]. Our static polarizabilities of the Yb atom and Yb<sup>+</sup> ion,  $143.9a_0^3$  and  $63.6a_0^3$ , also are in very good agreement with the most sophisticated atomic calculations, giving  $141 \pm 6a_0^3$  [61] and  $62.04a_0^3$  [42], respectively.

The potential-energy curves for the ground and excited states of the (LiYb)<sup>+</sup> molecular ion are presented in Fig. 2, and the spectroscopic characteristics are reported in Table I. The transition and permanent electric dipole moments are plotted in Figs. 3 and 4, respectively. The leading long-range coefficients for the dispersion and induction interactions between the Li<sup>+</sup> ion and the Yb atom and between the Yb<sup>+</sup> ion and the Li atom, all in the ground electronic state, are reported in Table II.

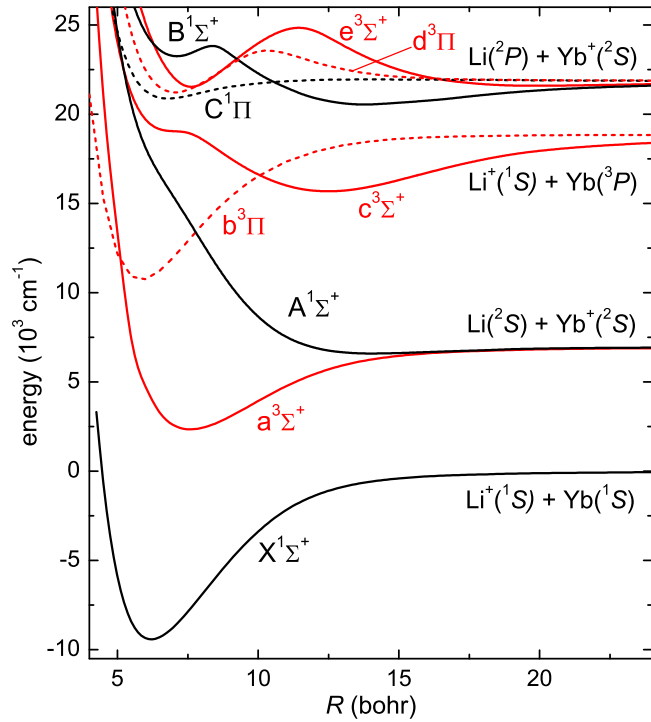


FIG. 2. (Color online) Nonrelativistic potential-energy curves of the  $(\text{LiYb})^+$  molecular ion.

The interaction of the ground-state  $\text{Li}^+$  ion with a ground-state ytterbium atom results in a single electronic state—the  $X^1\Sigma^+$  electronic ground state of the  $(\text{LiYb})^+$  molecular ion; cf. Fig. 2. The interaction between ion and atom is dominated by the induction contribution, resulting in the large binding energy of  $9412\text{ cm}^{-1}$ , with the equilibrium distance equal to 6.2 bohrs. The interaction of the ground-state  $\text{Yb}^+$  ion with a ground-state Li atom, which both are open shell, results in the two electronic states  $a^3\Sigma^+$  and  $A^1\Sigma^+$ . The triplet state is strongly bound with binding energy equal to

TABLE I. Spectroscopic characteristics of the  $(\text{LiYb})^+$  molecular ion: equilibrium bond lengths  $R_e$ , well depths  $D_e$ , harmonic constants  $\omega_0$ , and rotational constants  $B_0$  (for the isotope  $^7\text{Li}^{172}\text{Yb}^+$ ).

State	$R_e$ (bohr)	$D_e$ ( $\text{cm}^{-1}$ )	$\omega_0$ ( $\text{cm}^{-1}$ )	$B_0$ ( $\text{cm}^{-1}$ )
$X^1\Sigma^+$	6.20	$\text{Li}^+(^1S) + \text{Yb}(^1S)$ :	9412	231
		$\text{Li}(^1S) + \text{Yb}^+(^2S)$ :	358	37.1
$A^1\Sigma^+$	14.04	358	37.1	0.045
$a^3\Sigma^+$	7.59	4609	140	0.16
$b^3\Pi$	5.83	$\text{Li}^+(^1S) + \text{Yb}(^3P)$ :	8130	232
		$\text{Li}(^2P) + \text{Yb}^+(^2S)$ :	1332	50.1
$c^3\Sigma^+$	12.46	3177	60.9	0.057
$B^1\Sigma^+$	14.02	1332	50.1	0.045
$C^1\Pi$	6.71	1025	138	0.20
$e^3\Pi$	7.05	640	170	0.18
$d^3\Sigma^+$	7.56	426	218	0.16
$d^3\Sigma^+$	19.93	267	24.4	0.022

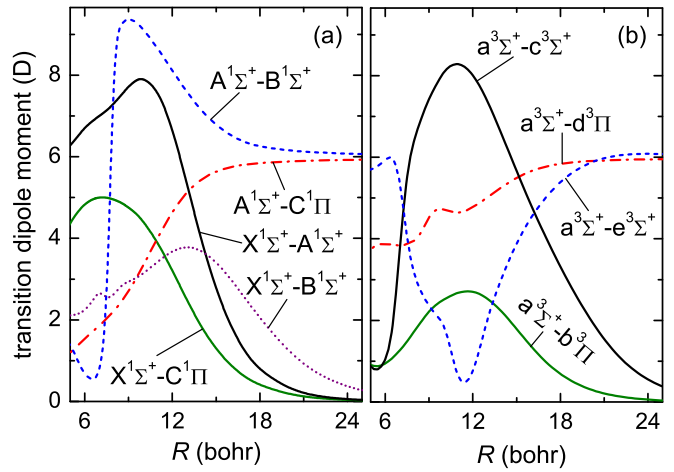


FIG. 3. (Color online) Transition electric dipole moments between singlet (a) and triplet (b) states of the  $(\text{LiYb})^+$  molecular ion.

$4609\text{ cm}^{-1}$ , whereas the singlet potential is weakly bound by only  $358\text{ cm}^{-1}$ . The large binding energy of the triplet  $a$  state as compared to that of the singlet  $A$  state can be rationalized in the molecular orbitals picture: The triplet  $a$  state is stabilized by an admixture of the antibonding orbital correlated to the lowest asymptote. While the order of the  $\text{LiYb}^+$  molecular states is the same as for the alkali-metal dimers, unlike in alkali-metal dimers the singlet ground state and the lowest triplet state are connected to different asymptotes. Thus the singlet  $A$  state, which is the first excited singlet state, corresponds to excited configurations with higher energies than the  $a$  state, and therefore it is weakly bound.

Estimating the uncertainty of *ab initio* calculations is a difficult task, especially for heavy many-electron systems. The accuracy depends on the proper treatment of relativistic effects, reproduction of the correlation energy, and convergence in the

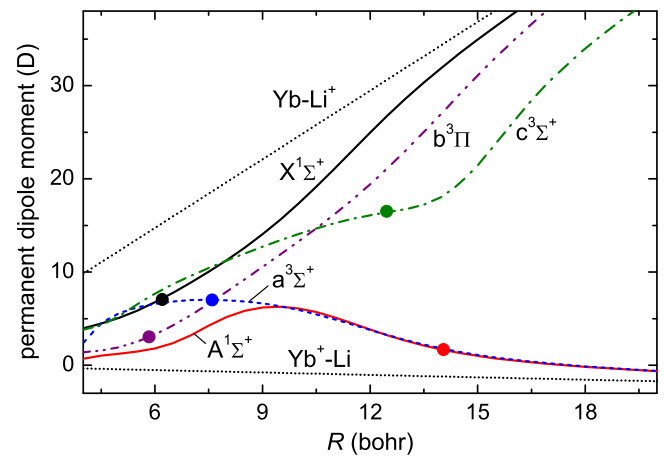


FIG. 4. (Color online) Permanent electric dipole moments of the most relevant singlet and triplet states of the  $(\text{LiYb})^+$  molecular ion. The  $z$  axis is oriented from Yb to Li and the origin is in the center of mass. The points indicate the values for the ground rovibrational level, and the dotted lines represent the permanent dipole moment that the molecular ion would have if the charge was completely localized on one of the atoms.



TABLE II. Induction and dispersion coefficients describing the long-range part of the interaction potential between the  $\text{Li}^+$  ion and the  $\text{Yb}$  atom and between the  $\text{Yb}^+$  ion and the  $\text{Li}$  atom, all in the ground electronic state.

System	$C_4^{\text{ind}}$ (units of $E_h a_0^4$ )	$C_6^{\text{ind}}$ (units of $E_h a_0^6$ )	$C_6^{\text{disp}}$ (units of $E_h a_0^6$ )
$\text{Li}^+ + \text{Yb}$	72.0	1280	6.4
$\text{Yb}^+ + \text{Li}$	82.1	711.7	711

size of the set of basis functions. The method employed here, including the relativistic pseudopotential and the basis sets used, are of the same quality as those reproducing the potential well depths of the lowest electronic states of the  $\text{Rb}_2$  [62] and  $\text{Sr}_2$  [28] molecules with an error of 3.5% or better as compared to experimental results. Based on this as well as additional convergence analysis for the present system, we estimate the total uncertainty of the calculated potential-energy curves for the lowest two asymptotes to be about 5% and somewhat larger for the higher excited states. The recently available theoretical predictions of the potential well depths of the lowest two singlet electronic states of the  $(\text{LiYb})^+$  molecular ion [63] agree with our results well within 28 and  $144 \text{ cm}^{-1}$  for the  $X^2\Sigma^+$  and  $A^2\Sigma^+$  states, respectively. The uncertainty of the calculated  $C_4$  and  $C_6$  coefficients, based on the accuracy of the used polarizabilities, is at most 5%.

Experimental proposals to immerse a ground-state ytterbium ion in a gas of ultracold ground-state lithium atoms rely on negligible losses due to the atom-ion interaction. In this respect, our electronic structure results, Fig. 2, are promising since the corresponding electronic states,  $a^3\Sigma^+$  and  $A^1\Sigma^+$ , are well separated from all other electronic states. This suggests that potential losses due to inelastic charge-transfer collisions should be smaller than those predicted and observed in ultracold collisions of a  $\text{Ba}^+$  ion with  $\text{Rb}$  atoms where strong spin relaxation was observed due to the spin-orbit coupling of both the incoming singlet  $A^1\Sigma^+$  and triplet  $a^3\Sigma^+$  states with the  $b^3\Pi$  state at short internuclear separation [6,7,29].

The value of the permanent electric dipole moments calculated with respect to the center of mass and presented in Fig. 4 increases with internuclear distance. This is typical for heteronuclear molecular ions. It implies that, in contrast to neutral molecules, even very weakly bound molecular ions will have a significant permanent electric dipole moment. The dotted lines in Fig. 4 represent the two limiting cases where the charge is completely localized on one of the atoms. The difference between the dotted lines and the calculated values can be understood as the interaction-induced variation of the permanent dipole moment [64] or the degree of charge delocalization. Asymptotically, the permanent dipole moments for all electronic states have to approach one of the two limiting cases.

## B. Elastic collisions

*Ab initio* electronic structure calculations do not provide sufficiently accurate interaction potentials to predict scattering lengths. We therefore calculate the scattering properties for a few isotopic mixtures with correspondingly different

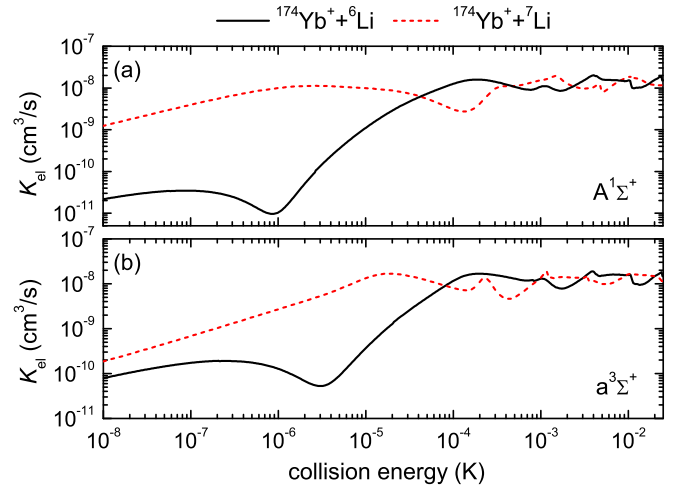


FIG. 5. (Color online) Elastic-scattering rates for collisions in the  $A^1\Sigma^+$  (a) and  $a^3\Sigma^+$  (b) electronic states. The  $^{174}\text{Yb}^+ + ^6\text{Li}$  isotope (black solid lines) corresponds to small background scattering length, the  $^{174}\text{Yb}^+ + ^7\text{Li}$  isotope (red dashed lines) to a large one.

scattering lengths. For our *ab initio* data, the low-energy  $s$ -wave scattering length in the  $A^1\Sigma^+$  ( $a^3\Sigma^+$ ) state amounts to  $-385a_0$  ( $-695a_0$ ) for  $^{174}\text{Yb}^+ + ^6\text{Li}$  and to  $2625a_0$  ( $982a_0$ ) for  $^{174}\text{Yb}^+ + ^7\text{Li}$ . For  $^{173}\text{Yb}^+ + ^6\text{Li}$  and  $^{173}\text{Yb}^+ + ^7\text{Li}$  the low-energy  $s$ -wave scattering length in the  $A^1\Sigma^+$  ( $a^3\Sigma^+$ ) state amounts to  $-371a_0$  ( $-659a_0$ ) and  $2705a_0$  ( $1042a_0$ ), respectively. These numbers have to be compared to the characteristic length scale of the atom-ion interaction [65,66] which is given by  $\sqrt{2\mu C_4/\hbar}$  and amounts to  $1218a_0$  for  $(\text{LiYb})^+$ . Therefore, the  $^{174}\text{Yb}^+ + ^6\text{Li}$  isotope corresponds to a small background scattering length and  $^{174}\text{Yb}^+ + ^7\text{Li}$  to a large one.

Elastic collision rate constants are reported in Fig. 5. The height of the centrifugal barrier, for an interaction potential varying as  $-C_4/r^4$ , is given by  $[(l+1)l]^{5/2}/(4C_4^{3/2}\mu^{5/2})$ . For example, the barrier height amounts to  $8.5 \mu\text{K}$  for  $p$ -wave collisions. For collision energies larger than  $10 \mu\text{K}$ , when more partial waves contribute to the scattering process, the total rate of elastic collisions is similar for all isotopic mixtures, of the order of  $10^{-8} \text{ cm}^3/\text{s}$ ; cf. Fig. 5. At lower energies, the elastic collision rates are decreased by two to three orders of magnitude and depend strongly on scattering length and spin symmetry. Specifically the scattering length and elastic collision rates in the Wigner regime depend on the hyperfine levels of colliding atoms and can be controlled by tuning magnetic Feshbach resonances that we will discuss in Sec. III F. Sympathetic cooling is likely to be possible if the ratio of the rates for elastic to all inelastic or reactive collisions is larger than roughly a factor of 100. The rates for all inelastic processes are reported in the following sections.

## C. Radiative charge transfer and radiative association

The  $A^1\Sigma^+$  electronic state is directly coupled to the ground  $X^1\Sigma^+$  electronic state by the electric transition dipole moment. This coupling is responsible for potential inelastic losses due

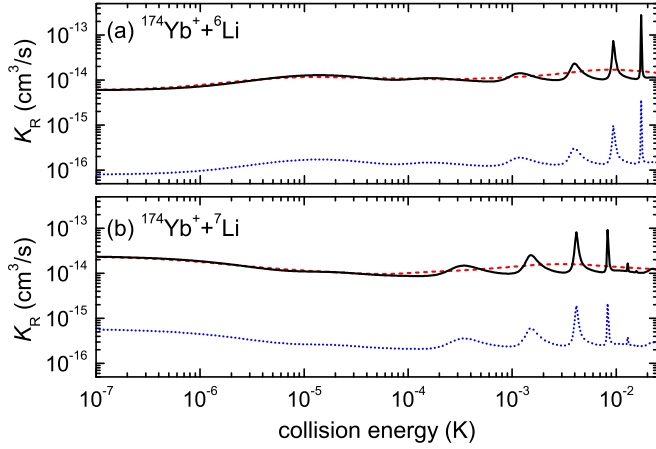
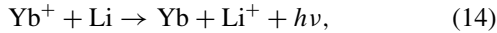
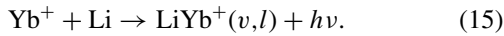


FIG. 6. (Color online) Rates for radiative association (black solid lines) and radiative charge transfer (blue dotted lines) for collisions of an  $^{174}\text{Yb}^+$  ion with  $^6\text{Li}$  and  $^7\text{Li}$  atoms. The red dashed envelopes are the thermally averaged rates.

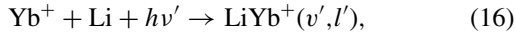
to spontaneous radiative charge transfer (CT),



or radiative association (RA),



It can also be used for laser-induced molecule formation, i.e., photoassociation (PA),



to the singlet state. The  $a^3\Sigma^+$  state is coupled by the electric transition dipole moment to the  $b^3\Pi$  and  $c^3\Sigma^+$  excited states. These couplings can be used for photoassociation to the triplet states.

Figure 6 presents the rate constants for radiative losses in collisions of the  $^{174}\text{Yb}^+$  ion with  $^6\text{Li}$  and  $^7\text{Li}$  atoms in the  $A^1\Sigma^+$  electronic state (in a field-free case where all spin orientations are present, the expected rate coefficients are only 25% of given values). The rates depend on the presence of resonances in the entrance channel and follow the Wigner threshold law for small collision energies and the Langevin limit for large collision energies. With rate constants two orders of magnitude larger than for radiative charge transfer, radiative association represents the main source of radiative loss that is a common feature for ultracold atom-ion systems [53,63,65–67]. At the same time, the rates for radiative loss are comparatively small,  $10^3$ – $10^5$  times smaller than the rates for the elastic scattering for temperatures below 10 mK; cf. Fig. 5. Radiative losses can further be reduced by several orders of magnitude by applying an external magnetic field which restricts the collisional dynamics of the  $\text{Yb}^+$  ion and the Li atom to the high-spin  $a^3\Sigma^+$  state. Since there is no radiative loss channel for the triplet state, the only radiative losses for collisions in magnetic field will originate from an admixture of the  $A^1\Sigma^+$  state. For an electronic state with a spin-stretched reference function, the admixture of a singlet state is given by the long-range dipolar spin-spin interaction and the spin-orbit coupling with higher excited states. Both appear in second order of perturbation theory, so they are very

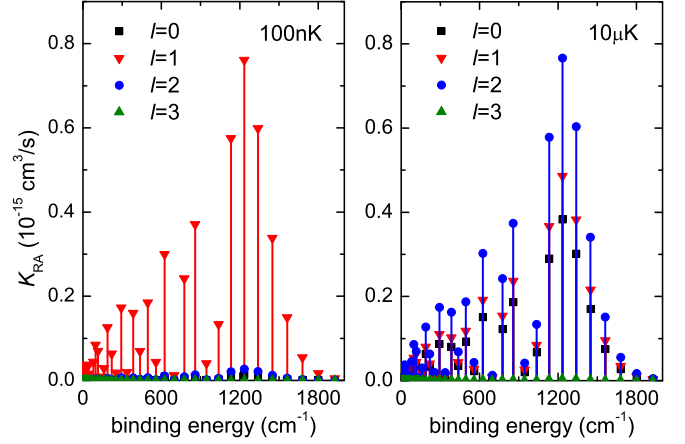


FIG. 7. (Color online) Radiative association rate vs binding energy of the final vibrational level in the  $X^1\Sigma^+$  ground electronic state for an  $^{174}\text{Yb}^+$  ion colliding with a  $^6\text{Li}$  atom in the  $A^1\Sigma^+$  state plotted at a temperature corresponding to 100 nK (left panel) and to  $10\ \mu\text{K}$  (right panel).

small [45,46]. For these reasons, radiative losses should not pose a problem for sympathetic cooling of  $\text{Yb}^+$  ions by a gas of ultracold Li atoms, especially if an external magnetic field is applied.

Radiative association is further analyzed in Fig. 7 which shows the RA rates to different rovibrational levels of the  $(^6\text{Li}^{174}\text{Yb})^+$  molecular ion at temperatures of  $T = 100\ \text{nK}$  and  $10\ \mu\text{K}$ . As expected, at low temperatures the radiative association is dominated by the contribution of  $s$ -wave collisions, whereas at higher temperatures more partial waves come into play. The RA spectra for other isotopes have very similar shapes as those shown in Fig. 7 but the amplitudes of the rates vary due to actual value of the scattering length and the presence of resonances in the entrance channel. Interestingly, the largest partial rates are found for relatively strongly bound vibrational levels with binding energies of about  $1200\ \text{cm}^{-1}$ . The position of the maximum in the radiative association spectrum results from the interplay of the overlaps between initial scattering and exit vibrational states (related to the structure of electronic states, Fig. 2) and the electric transition dipole moment that decays at large internuclear distances, Fig. 3(a). Spontaneous radiative association can thus be used to produce  $(\text{LiYb})^+$  molecular ions. In Secs. III E and III F below, we will show that the molecule formation rates can be controlled by means of a laser field in photoassociation or by a magnetic field modifying Feshbach resonances. The latter is similar to Feshbach-optimized photoassociation of neutral molecules [68]. But before investigating the control of atom-ion collisions by external fields, we examine the sensitivity of our predictions for elastic and inelastic cross sections on the interaction potential, in particular on the scattering length.

#### D. Sensitivity to the interaction potential

Even the best state of the art *ab initio* methods cannot provide a reliable estimate of the  $s$ -wave scattering length for many-electron atoms. Since for  $(\text{LiYb})^+$ , the  $s$ -wave scattering

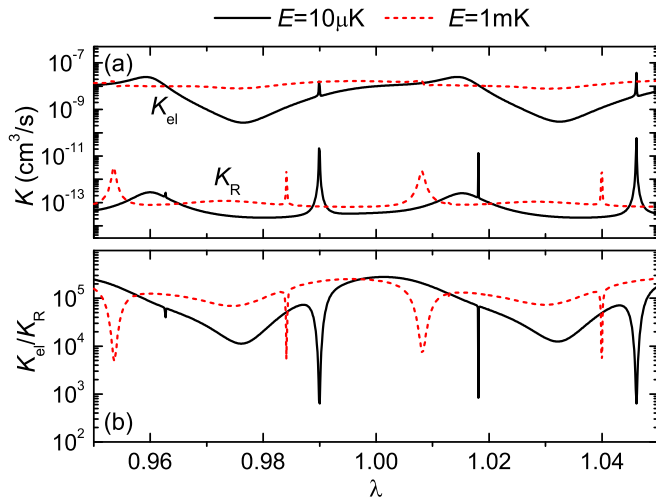


FIG. 8. (Color online) Sensitivity of the rate constants for elastic scattering  $K_{\text{el}}$  and radiative association and charge transfer  $K_{\text{R}}$  (a) and of the ratio of elastic to inelastic rate constants (b) at collision energies of  $10 \mu\text{K}$  (black solid lines) and  $1 \text{ mK}$  (red dashed lines) to a scaling factor  $\lambda$  applied to the interaction potential,  $V(R) \rightarrow \lambda V(R)$ .

length has not yet been measured, it is important to assess the dependency of our results on this quantity. Most severely, a different value of the scattering length than that obtained with our data might compromise our conclusions for sympathetic cooling. Comparison of Figs. 5 and 6 suggests sympathetic cooling to be feasible since the elastic cross section is three to five orders of magnitude larger than the cross section for all inelastic processes in the relevant temperature range. If the true background scattering length is very small, smaller than that for  $^{174}\text{Yb} + ^6\text{Li}$  (red dashed lines in Fig. 5 and upper panel of Fig. 6), the elastic rate constant will be smaller. At the same time the inelastic losses will also be smaller, due to the decreased amplitude of the scattering wave function in the entrance channel. This can be estimated, for example, using Eq. (25) of Ref. [29]. As a result, even for scattering lengths smaller than that of  $^{174}\text{Yb} + ^6\text{Li}$  in our calculations, the ratio of elastic to inelastic rate constants should still be of the order of at least 100 for temperatures between  $10 \text{ nK}$  and  $10 \text{ mK}$ . For higher temperatures, when many partial waves contribute, the overall rate constant is less dependent on the  $s$ -wave scattering length unless a broad shape resonance appears. The recently available theoretical results on the radiative charge transfer and radiative association in the  $\text{Li} + \text{Yb}^+$  system [63] reproduce our overall energy dependence and the order of magnitude of the rate constants.

For a more detailed assessment of the sensitivity of our results on the uncertainty of the scattering length, we follow the approach employed in, among others, Refs. [69–71]. Specifically, we have carried out calculations with the interaction potential scaled by a factor  $\lambda$ , taking values in the range  $0.95$ – $1.05$ . This scaling roughly corresponds to the estimated error bounds in the calculated potential-energy curves and changes the number of bound states by  $\mp 1$ . The results are shown in Fig. 8 for collision energies of  $10 \mu\text{K}$  and  $1 \text{ mK}$ . Inspection of Fig. 8 reveals a weak dependence of the cross sections on the potential scaling factor  $\lambda$  to only be interrupted

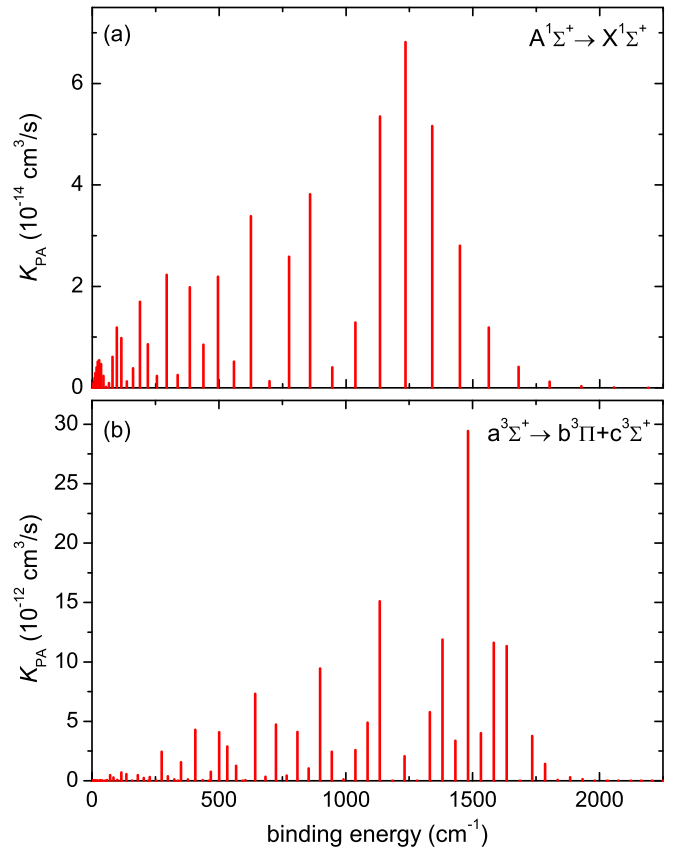


FIG. 9. (Color online) Photoassociation rates for rovibrational levels in the  $X^1\Sigma^+$  ground electronic state and  $A^1\Sigma^+$  state collisions of  $^{174}\text{Yb}^+$  ions with  $^6\text{Li}$  atoms (upper panel) and for rovibrational levels in the  $c^3\Sigma^+$  and  $b^3\Pi$  states and  $a^3\Sigma^+$  state collisions (lower panel) for a laser intensity of  $I = 100 \text{ W/cm}^2$  and a temperature of  $10 \mu\text{K}$ .

by the presence of sharp resonances that occur when bound states of  $(\text{LiYb})^+$  cross the incoming threshold as a function of  $\lambda$ . According to Fig. 8, these resonances occur in narrow ranges of  $\lambda$ . The probability that the true potential will be such that the ratio of elastic to inelastic cross sections is seriously affected is therefore quite small. Last but not least, the ratio of elastic to inelastic cross section is always much larger than 100. Within the grid of  $\lambda$  employed in the present calculations, we thus find strong evidence that sympathetically cooling an  $\text{Yb}^+$  ion by laser-cooled  $\text{Li}$  atoms is possible. It is worth noting that the effect of resonances on the rate constants will be additionally washed out by Boltzmann averaging [72]. The statement predicting feasibility of sympathetic cooling can be made even stronger by exploiting the magnetic-field dependence of the scattering length, discussed in Sec. III F.

### E. Photoassociation

Photoassociation refers to the controlled formation of molecules by applying a laser field [73] and is also a useful tool, e.g., for spectroscopic investigations.  $(\text{LiYb})^+$  molecular ions can be produced in either singlet or triplet states: If the colliding  $\text{Yb}^+$  ion and  $\text{Li}$  atom interact via the  $A^1\Sigma^+$  electronic state, photoassociation to the  $X^1\Sigma^+$  state is in

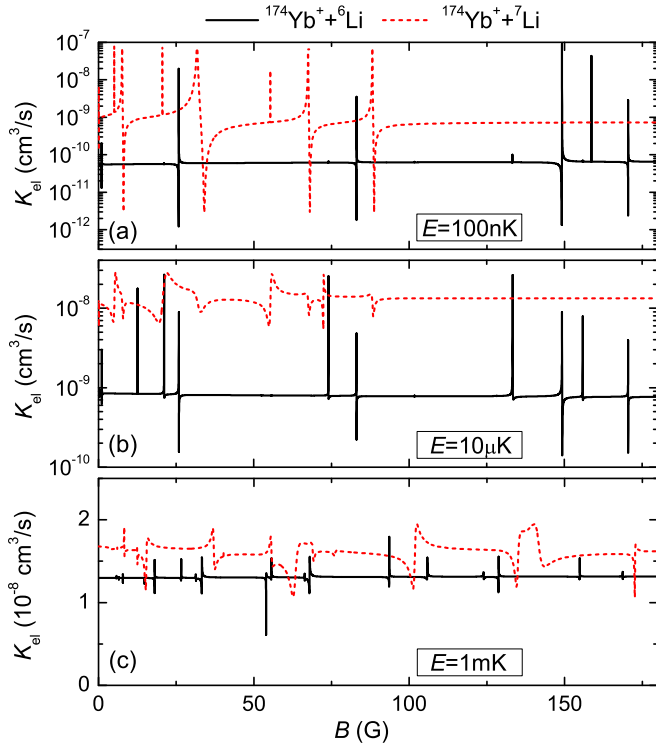


FIG. 10. (Color online) Elastic-scattering rate constant vs magnetic field for collisions of fermionic  $^{174}\text{Yb}^+(\frac{1}{2}, -\frac{1}{2})$  ions with  $^6\text{Li}(\frac{1}{2}, \frac{1}{2})$  atoms and  $^7\text{Li}(1, 1)$  atoms for collision energies corresponding to 100 nK, 10  $\mu\text{K}$ , and 1 mK. Note the different y-axis scales.

principle possible for laser wavelengths between 611 and 1438 nm. However, in practice the photoassociation window is to a wavelength between 1050 and 1438 nm due to unfavorable Franck-Condon factors. If the atom and ion are in the  $a^3\Sigma^+$  state, photoassociation into the manifold of the  $b^3\Pi$  and  $c^3\Sigma^+$  states can be induced with laser wavelengths between 834 and 1140 nm. Since the triplet molecules are formed in an electronically excited state, they are subject to comparatively fast spontaneous decay, whereas the singlet molecules in the electronic ground state are more stable.

Photoassociation spectra for  $^6\text{Li};^{174}\text{Yb}^+$  are presented in Figs. 9(a) and 9(b) for the singlet and triplet spin symmetries, respectively. In both cases, and similarly to the radiative association discussed above, relatively strongly bound rovibrational levels can be populated, with binding energies of about 1200  $\text{cm}^{-1}$  (1500  $\text{cm}^{-1}$ ) for the singlet (triplet) symmetry. The overall shape of the photoassociation spectrum for the singlet symmetry is, as expected, similar to the radiative association spectrum presented in Fig. 7. It is not possible to produce singlet state  $(\text{LiYb})^+$  molecular ions with larger binding energy by using a one-photon transition since the  $A^1\Sigma^+$  electronic state is repulsive at the equilibrium distance of the  $X^1\Sigma^+$  ground electronic state. To access the  $X^1\Sigma^+$  ground vibrational level, additional Raman transfer would be necessary.

For triplet state  $(\text{LiYb})^+$  molecular ions, the largest photoassociation rates are found for ions with a dominant  $c^3\Sigma^+$  state component close to the equilibrium internuclear distance. The formation of triplet molecules dominated by the  $b^3\Pi$

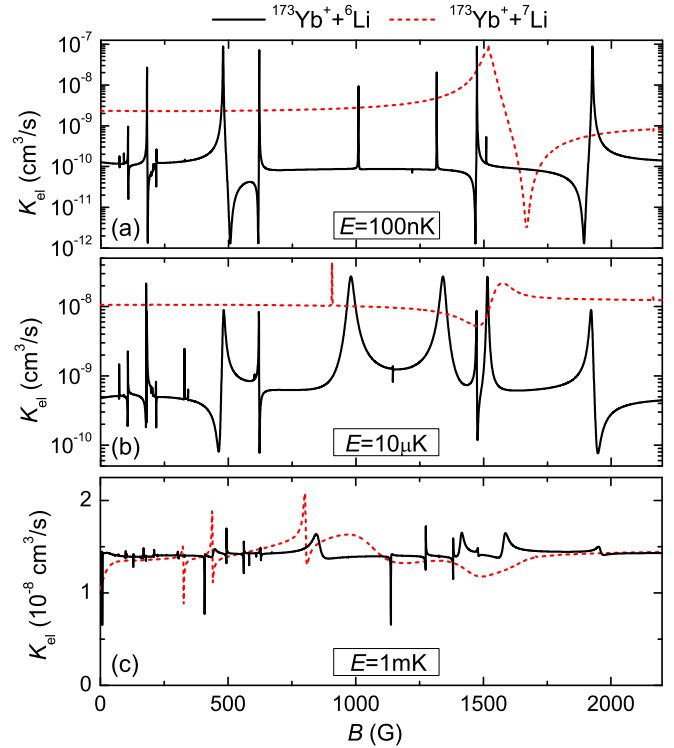


FIG. 11. (Color online) Elastic-scattering rate vs magnetic field for collisions of bosonic  $^{173}\text{Yb}^+(3, -3)$  ions with  $^6\text{Li}(\frac{1}{2}, \frac{1}{2})$  atoms and  $^7\text{Li}(1, -1)$  atoms for collision energies corresponding to 100 nK, 10  $\mu\text{K}$ , and 1 mK.

state component close to the equilibrium internuclear distance (with a binding energy of about 7000  $\text{cm}^{-1}$ ) is possible. But the rates for these transitions are three orders of magnitude smaller than the rates for transitions to the levels dominated by the  $c^3\Sigma^+$  state component. The lifetime of triplet excited-state molecules is limited by spontaneous decay. Longer lived molecules in the  $a^3\Sigma^+$  state can be obtained by either spontaneous or stimulated emission. These molecules can also be state-selectively produced in one step using stimulated Raman adiabatic passage (STIRAP).

The PA spectra for other isotopes have very similar shapes as those shown in Fig. 9 but the amplitudes of the rates vary due to actual value of the scattering length and the presence of resonances in the entrance channel. It is worth noting that the characteristics of the spectra for photoassociation to the lowest singlet and triplet states of  $(\text{LiYb})^+$  presented in Fig. 9, in particular the maxima for relatively deeply bound molecules, are common for all ion-atom systems when both atom and ion are in the  $^2S$  electronic ground state. This is in contrast to the photoassociation of alkali-metal atoms in the  $^2S$  electronic ground state which leads to weakly bound molecules.

The controlled formation of molecular ions is feasible only if the photoassociation rate (Fig. 9) is larger than the rates for radiative losses (Fig. 7). For the investigated system of  $\text{Yb}^+$  ion and Li atom, this condition is met. Additionally, the photoassociation rate can be enhanced by controlling magnetic Feshbach resonances [68] which are investigated in the next section.



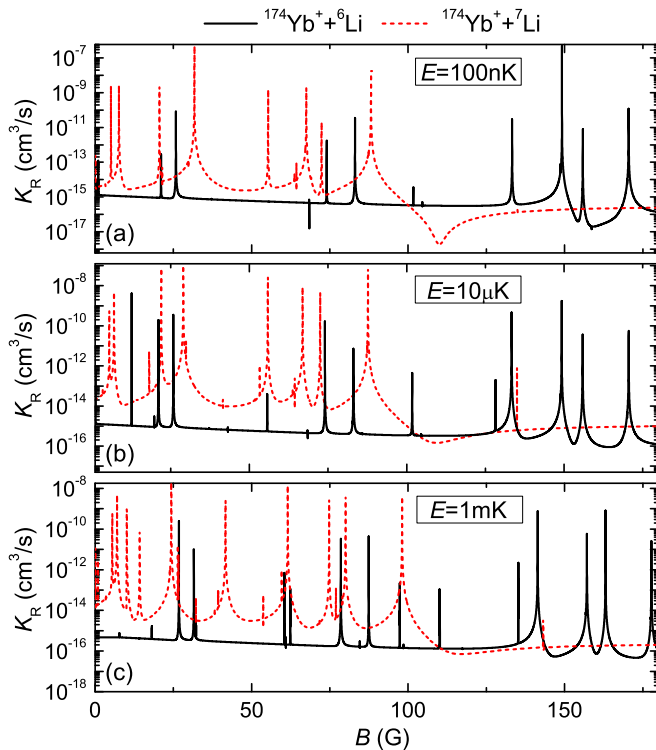


FIG. 12. (Color online) Radiative loss rate vs magnetic field for collisions between  $^{174}\text{Yb}^+(\frac{1}{2}, -\frac{1}{2})$  ions and  $^6\text{Li}(\frac{1}{2}, \frac{1}{2})$ , respectively,  $^7\text{Li}(1, 1)$  atoms for collision energies corresponding to 100 nK, 10  $\mu\text{K}$ , and 1 mK.

### F. Feshbach resonances

Two types of magnetically tunable Feshbach resonances between the  $\text{Yb}^+$  ion and the Li atom exist, depending on the structure of the  $\text{Yb}^+$  ion: (i) Fermionic  $\text{Yb}^+$  ions do not have nuclear spin and therefore they do not possess any hyperfine structure. Feshbach resonances between fermionic  $\text{Yb}^+$  ions and Li atoms result from the interaction of the hyperfine structure of the Li atom with the electronic spin of the  $\text{Yb}^+$  ion [65,66]. (ii) Bosonic  $\text{Yb}^+$  ions ( $^{171}\text{Yb}^+$  and  $^{173}\text{Yb}^+$ ) have a nonzero nuclear spin. As a consequence, they possess a hyperfine manifold, such that Feshbach resonances between bosonic  $\text{Yb}^+$  ions and Li atoms are of the same nature as those between two alkali-metal atoms [74]. The density of the Feshbach resonances at small magnetic fields in the former case is larger compared to the latter case; cf. Figs. 10 and 11. Note the different  $x$ -axis scales for the magnetic field in Figs. 10 and 11. The impact of the Lorentz force and Landau quantization effects [75] is neglected in the present study.

Figure 10 shows the rates for the elastic scattering of the fermionic  $^{174}\text{Yb}^+$  ion in the  $(f, m_f) = (\frac{1}{2}, -\frac{1}{2})$  state with fermionic  $^6\text{Li}(\frac{1}{2}, \frac{1}{2})$  and bosonic  $^7\text{Li}(1, 1)$  atoms for collision energies corresponding to 100 nK, 10  $\mu\text{K}$ , and 1 mK as a function of the external magnetic field. Contributions from the lowest 3, 7, and 15 partial waves are included, respectively, at these three energies. The density of Feshbach resonances for the fermionic  $^6\text{Li}$  atom is larger compared to bosonic  $^7\text{Li}$  because the fermionic atom has a smaller hyperfine splitting than

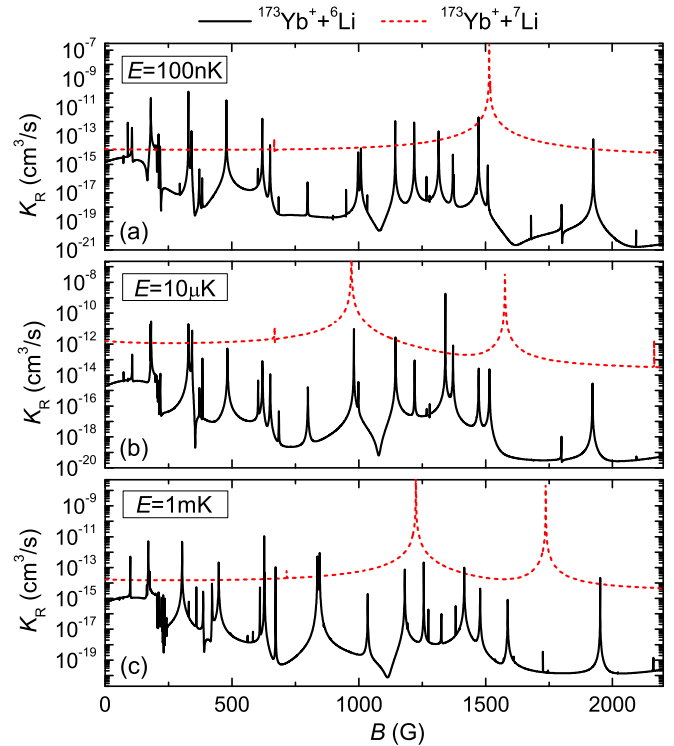


FIG. 13. (Color online) Radiative loss rate vs magnetic field for collisions between  $^{173}\text{Yb}^+(3, -3)$  ions and  $^6\text{Li}(\frac{1}{2}, \frac{1}{2})$ , respectively,  $^7\text{Li}(1, -1)$  atoms for collision energies corresponding to 100 nK, 10  $\mu\text{K}$ , and 1 mK.

the bosonic one, 228.2 MHz versus 803.5 MHz. The scattering at temperatures of 100 nK is dominated by  $s$ -wave collisions. The large Feshbach resonances visible in Fig. 10(a) are almost pure  $s$ -wave resonances, whereas the very narrow resonances are of  $p$ -wave character. The widths of these resonances are relatively small, mostly below 1 G. At a temperature of 10  $\mu\text{K}$ ,  $s$ -wave and  $p$ -wave collisions contribute equally, cf. Fig. 10(b), and at temperatures above 100  $\mu\text{K}$ , more partial waves start to contribute to the elastic scattering. At a temperature of 1 mK, as presented in Fig. 10(c), the elastic scattering is dominated by higher partial waves ( $l = 3$  and  $l = 4$ ) which wash out the resonance structure of the lower partial waves. Thus the Feshbach resonances visible in Fig. 10(c) are narrower and have much smaller amplitude as compared to those at lower temperatures.

Elastic-scattering rates for bosonic  $^{173}\text{Yb}^+(3, -3)$  ions and fermionic  $^6\text{Li}(\frac{1}{2}, \frac{1}{2})$  atoms, respectively, bosonic  $^7\text{Li}(1, -1)$  atoms as a function of the external magnetic field, are shown in Fig. 11 for collision energies of 100 nK, 10  $\mu\text{K}$ , and 1 mK. Similarly to the case of the fermionic  $^{174}\text{Yb}^+$  ion, cf. Fig. 10, scattering at a temperature of 100 nK is dominated by  $s$ -wave collisions with a few narrow  $p$ -wave resonances visible. The widths of these resonances are of the order of a few to several G. At 10  $\mu\text{K}$ ,  $s$ -wave and  $p$ -wave collisions contribute equally and at temperatures above 1 mK many partial waves contribute to the rate of the elastic scattering. The structure and strength of the Feshbach resonances at temperatures above 1 mK is washed out by

dominant contributions of higher partial waves to the total elastic-scattering rate.

Finally, Figs. 12 and 13 present the rates for radiative losses, that is, radiative association and radiative charge transfer, as a function of magnetic field for collisions of the same species at the same temperatures as in Figs. 10 and 11. In contrast to the elastic-scattering rates, Feshbach and shape resonances are clearly visible for all investigated temperatures. Far from resonances the typical rates for elastic scattering are, as expected, at least three orders of magnitude larger than the rates for radiative losses.

Comparing Figs. 10 and 11 to Figs. 12 and 13, a different temperature dependence of the rates for elastic scattering and radiative losses is observed. This can be understood by analyzing the mechanisms of the two processes: The elastic rates are dominated by reflection from the long-range potential. For higher partial waves with a large centrifugal barrier which dominate at high collision energies, the appearance of Feshbach resonances is strongly suppressed. By contrast, radiative losses occur at short internuclear distance only. For high partial waves, this requires tunneling through the centrifugal barrier. The probability of tunneling decays exponentially with the height of the centrifugal barrier. Therefore, at higher temperatures, higher partial waves contribute less to the radiative losses than to elastic scattering.

For other isotopes, both fermionic and bosonic ones, the characteristics of Feshbach resonances, such as the density of resonances, the temperature dependence of elastic and inelastic cross sections, and the feasibility of controlling the ion-atom interaction with an external magnetic field, are similar to those discussed above. In particular, they depend on the choice of the entrance channel characterized by the hyperfine states of atom and ion and the scattering length. Different isotopes of Yb can be used to control the structure of Feshbach resonances due to the different masses. However, this control is somewhat limited since, due to the much smaller mass of the Li atom, the scattering length depends less on the mass of the Yb atom as compared to mass-balanced mixtures.

The magnetic-field dependence of the scattering length can be exploited to ensure the condition needed for sympathetic cooling. Figures 12 and 13 show minima in the radiative loss constants [76], for example close to 160 G in Fig. 12 (top and middle panels). Tuning the magnetic field to such a value will enhance the ratio of elastic to inelastic rate constants by a factor of 1000 and should yield very efficient sympathetic cooling. Another option consists in tuning the magnetic field close to one of the broader Feshbach resonances, observed in Figs. 10 and 11, to increase the elastic rate constant while keeping inelastic losses at bay. The exact positions of the Feshbach resonances will depend on the true value of the scattering length. However, the characteristics of the presented results, such as the density of resonances, are general and depend essentially on the hyperfine structure and nature of colliding ion and atom. We therefore expect our predictions to be valid, independent of the specific value of the background scattering length.

The magnetic-field dependence can also be employed to enhance the inelastic rate constants, in case one is interested in the observation of cold chemical reactions. If the field-free scattering length is essentially zero, this will decrease the

inelastic rate constants, as explained above. The remedy then is to tune the magnetic field to a value where a maximum in  $K_R$  is observed; cf. Figs. 12 and 13. Alternatively, one could also make use of minima in the elastic rate constants, cf. Fig. 10, which will decrease the ratio of the rate constants by up to a factor of 1000. The latter is not applicable at higher temperatures ( $> 10 \mu\text{K}$ ) where the Feshbach resonances are less pronounced in the elastic rate constant.

#### IV. SUMMARY AND CONCLUSIONS

We have carried out state-of-the-art *ab initio* calculations to determine the electronic structure of the  $(\text{LiYb})^+$  molecular ion. Potential-energy curves, transition and permanent electric dipole moments, and long-range coefficients were calculated. Good agreement between our computed atomic results and the available experimental data was obtained.

The entrance channels for collisions between the  $\text{Yb}^+(^2S)$  ion and the  $\text{Li}(^2S)$  atom are found to be well separated from all other electronic states, suggesting comparatively small losses due to reactive collisions. Significant permanent electric dipole moments are obtained, even for very weakly bound states of the molecular ion. This opens the way for various control schemes. For example, a nonresonant laser field will lead to a strong Stark effect that can be used to control energy-level shifts state-selectively. This should enable state-selective detection of the products of the atom-ion chemical reactions.

We have subsequently employed the electronic structure data to calculate the rate constants for elastic scattering as well as radiative charge transfer and radiative association with and without magnetic field. The relevant temperature scale is set by micromotion in the Paul trap. For  $\text{Li}+\text{Yb}^+$ , it is less severe than for other species due to the favorable ion to atom mass ratio, limiting the trap temperature to about  $10 \mu\text{K}$  [22–24]. At this temperature, we find clear signatures of Feshbach resonances. This suggests that it should be possible to observe these resonances and use them to control the atom-ion interactions, facilitating sympathetic cooling or molecule formation. This encouraging finding for  $\text{Yb}^+$  in the Paul trap, immersed in a gas of ultracold Li atoms, is in contrast to many other atom-ion species [65,66].

Temperatures lower than 10 mK require sympathetic cooling. Our results predict a sufficiently large ratio of elastic to inelastic scattering cross sections, and thus feasibility of sympathetic cooling, in the temperature range between 10 mK and  $10 \mu\text{K}$  for both small and large values of the scattering length. Prospects for sympathetic cooling all the way down to 10 nK for the ion trapped in an optical dipole trap also look good. However, at these very low temperatures, resonances may have a detrimental effect, and our predictions come with some uncertainty due to the unknown exact value of the scattering length. We have critically assessed the validity of our results by scaling the interaction potential, assuming an accuracy of the *ab initio* data of  $\pm 5\%$ . Except for extremely narrow ranges of the scaling factor, we find the ratio of elastic-to inelastic-scattering cross sections to be larger than 100. The probability that the true interaction potential corresponds to an unfavorable value of the scaling factor is very small, and such an unfortunate case could be remedied by changing the isotope. We are thus confident to predict feasibility of

sympathetic cooling of an  $\text{Yb}^+$  ion by Li atoms down to temperatures of about 10 nK. This implies excellent prospects for building a quantum simulator using  $\text{Yb}^+$  ions immersed in a gas of ultracold Li atoms, bringing quantum simulation of solid-state physics with atomic, molecular, optical physics (AMO) experiments a step closer to reality [16,17].

Moreover, since radiative association is found to dominate radiative inelastic processes,  $(\text{LiYb})^+$  is also a good candidate for observing ultracold atom-ion chemical reactions. *Controlled* formation of molecular ions becomes possible by applying a laser field, accessing vibrational levels in the ground electronic state as well as electronically excited triplet states. Photoassociation can utilize one-photon transitions to levels with moderate binding energies. The formation of molecular ions in their absolute ground state will require additional Raman transitions.

Our calculated photoassociation spectra are also important for optical trapping since they indicate that photoassociation losses are likely to occur at wavelengths close to 1064 nm. Since photoassociation lines are typically quite narrow, it should be possible to avoid these losses by proper tuning of the trapping laser. Our calculations indicate in which regions transitions are to be expected but would need to be corroborated by spectroscopy for quantitative predictions.

Molecular ions offer a particularly interesting perspective for photoassociation and related spectroscopies, in that state-selective detection of a single molecular ion in the trap should be possible. Such a detection scheme can be based on a change

of the trapping frequency due to the change of the ion mass when the bond is formed or broken. State selectivity could be achieved by exploiting the differences in the Stark shifts of different rovibrational levels which modify the spectrum of the trapped ion. One can thus envision a series of photoassociation and dissociation experiments, detected by changes in the fluorescence wavelength. Similarly, one can photoinduce, and potentially control, ion-neutral chemical reactions by laser excitation of Li into the  $^2P$  state. Due to the favorable shape of the corresponding  $^1\Pi$  state, this might provide an alternative and more direct route for producing molecular ions in their absolute ground state than photoassociation into the  $X^1\Sigma^+$  ground electronic state.

To conclude,  $\text{Li} + \text{Yb}^+$  represents an extremely promising example of hybrid atom-ion systems. Good prospects for sympathetic cooling should allow for its application in quantum simulation in the not too distant future [16,17], and several pathways to molecule formation imply interesting avenues for cold controlled chemical reactions.

#### ACKNOWLEDGMENTS

We would like to thank T. Calarco for bringing our attention to this problem and R. Gerritsma for useful discussions. M.T. and R.M. thank the Foundation for Polish Science for support within the START and MISTRZ programs, respectively; R.M. was supported by the Polish Ministry of Science and Higher Education through Project No. N204 215539.

- 
- [1] D. Leibfried, R. Blatt, C. Monroe, and D. Wineland, *Rev. Mod. Phys.* **75**, 281 (2003).
- [2] H. Häffner, C. F. Roos, and R. Blatt, *Phys. Rep.* **469**, 155 (2008).
- [3] R. Blatt and C. F. Roos, *Nat. Phys.* **8**, 277 (2012).
- [4] C. Zipkes, S. Palzer, C. Sias, and M. Köhl, *Nature (London)* **464**, 388 (2010).
- [5] C. Zipkes, S. Palzer, L. Ratschbacher, C. Sias, and M. Köhl, *Phys. Rev. Lett.* **105**, 133201 (2010).
- [6] L. Ratschbacher, C. Zipkes, C. Sias, and M. Köhl, *Nat. Phys.* **8**, 649 (2012).
- [7] L. Ratschbacher, C. Sias, L. Carcagni, J. M. Silver, C. Zipkes, and M. Köhl, *Phys. Rev. Lett.* **110**, 160402 (2013).
- [8] S. Schmid, A. Härter, and J. H. Denschlag, *Phys. Rev. Lett.* **105**, 133202 (2010).
- [9] A. T. Grier, M. Cetina, F. Oručević, and V. Vuletić, *Phys. Rev. Lett.* **102**, 223201 (2009).
- [10] A. Härter, A. Krütkow, A. Brunner, W. Schnitzler, S. Schmid, and J. H. Denschlag, *Phys. Rev. Lett.* **109**, 123201 (2012).
- [11] K. Ravi, S. Lee, A. Sharma, G. Werth, and S. Rangwala, *Nat. Commun.* **3**, 1126 (2012).
- [12] F. H. J. Hall, M. Aymar, N. Bouloufa-Maafa, O. Dulieu, and S. Willitsch, *Phys. Rev. Lett.* **107**, 243202 (2011).
- [13] W. G. Rellergert, S. T. Sullivan, S. Kotochigova, A. Petrov, K. Chen, S. J. Schowalter, and E. R. Hudson, *Phys. Rev. Lett.* **107**, 243201 (2011).
- [14] S. T. Sullivan, W. G. Rellergert, S. Kotochigova, and E. R. Hudson, *Phys. Rev. Lett.* **109**, 223002 (2012).
- [15] W. W. Smith, D. S. Goodman, I. Sivarajah, J. E. Wells, S. Banerjee, R. Côté, H. H. Michels, J. A. Montgomery, Jr., and F. A. Narducci, *Appl. Phys. B* **114**, 75 (2014).
- [16] R. Gerritsma, A. Negretti, H. Doerk, Z. Idziaszek, T. Calarco, and F. Schmidt-Kaler, *Phys. Rev. Lett.* **109**, 080402 (2012).
- [17] U. Bissbort, D. Cocks, A. Negretti, Z. Idziaszek, T. Calarco, F. Schmidt-Kaler, W. Hofstetter, and R. Gerritsma, *Phys. Rev. Lett.* **111**, 080501 (2013).
- [18] F. H. J. Hall and S. Willitsch, *Phys. Rev. Lett.* **109**, 233202 (2012).
- [19] C. Schneider, M. Enderlein, T. Huber, and T. Schaetz, *Nat. Photon.* **4**, 772 (2010).
- [20] C. Cormick, T. Schaetz, and G. Morigi, *New J. Phys.* **13**, 043019 (2011).
- [21] W. Paul, *Rev. Mod. Phys.* **62**, 531 (1990).
- [22] M. Cetina, A. T. Grier, and V. Vuletić, *Phys. Rev. Lett.* **109**, 253201 (2012).
- [23] K. Chen, S. T. Sullivan, and E. R. Hudson, *Phys. Rev. Lett.* **112**, 143009 (2014).
- [24] M. Krych and Z. Idziaszek, *Phys. Rev. A* **91**, 023430 (2015).
- [25] Note that while our paper was under review, another study has become available [63].
- [26] R. Gerritsma (private communication).
- [27] M. Tomza, F. Pawłowski, M. Jeziorska, C. P. Koch, and R. Moszynski, *Phys. Chem. Chem. Phys.* **13**, 18893 (2011).
- [28] W. Skomorowski, F. Pawłowski, C. P. Koch, and R. Moszynski, *J. Chem. Phys.* **136**, 194306 (2012).

- [29] M. Krych, W. Skomorowski, F. Pawłowski, R. Moszynski, and Z. Idziaszek, *Phys. Rev. A* **83**, 032723 (2011).
- [30] R. J. Bartlett and M. Musial, *Rev. Mod. Phys.* **79**, 291 (2007).
- [31] P. J. Knowles, C. Hampel, and H.-J. Werner, *J. Chem. Phys.* **99**, 5219 (1993).
- [32] O. Christiansen, H. Koch, and P. Jorgensen, *J. Chem. Phys.* **103**, 7429 (1995).
- [33] H. Koch, O. Christiansen, P. Jorgensen, A. M. S. de Meras, and T. Helgaker, *J. Chem. Phys.* **106**, 1808 (1997).
- [34] S. Boys and F. Bernardi, *Mol. Phys.* **19**, 553 (1970).
- [35] H.-J. Werner, P. J. Knowles, F. R. M. R. Lindh, M. Schütz, P. Celani, T. Korona, G. Rauhut, R. D. Amos, A. Bernhardsson, A. Berning, D. L. Cooper, M. J. O. Deegan, A. J. Dobbyn, E. G. F. Eckert, C. Hampel, G. Hetzer, A. W. Lloyd, S. J. McNicholas, W. Meyer, M. E. Mura, A. Nicklass, P. Palmieri, R. Pitzer, U. Schumann, H. Stoll, A. J. Stone, R. Tarroni, T. Thorsteinsson, M. Wang, and A. Wolf, MOLPRO, version 2012.1, a package of *ab initio* programs, 2012; see <http://www.molpro.net>.
- [36] T. Helgaker, H. J. A. Jensen, P. Jorgensen, J. Olsen, K. Ruud, H. Agren, A. A. Auer, K. L. Bak, V. Bakken, O. Christiansen *et al.*, DALTON, an *ab initio* electronic structure program, release 2.0, 2005.
- [37] I. S. Lim, H. Stoll, and P. Schwerdtfeger, *J. Chem. Phys.* **124**, 034107 (2006).
- [38] B. Jeziorski and R. Moszynski, *Int. J. Quantum Chem.* **48**, 161 (1993).
- [39] R. Moszynski, P. Zuchowski, and B. Jeziorski, *Collect. Czech. Chem. Commun.* **70**, 1109 (2005).
- [40] T. Korona, M. Przybytek, and B. Jeziorski, *Mol. Phys.* **104**, 2303 (2006).
- [41] A. Derevianko, S. G. Porsev, and J. F. Babb, *At. Data Nucl. Data Tables* **96**, 323 (2010).
- [42] U. I. Safronova and M. S. Safronova, *Phys. Rev. A* **79**, 022512 (2009).
- [43] C. Chen and Z.-W. Wang, *J. Chem. Phys.* **121**, 4171 (2004).
- [44] S. G. Porsev, M. S. Safronova, A. Derevianko, and C. W. Clark, *Phys. Rev. A* **89**, 012711 (2014).
- [45] H. T. C. Stoof, J. M. V. A. Koelman, and B. J. Verhaar, *Phys. Rev. B* **38**, 4688 (1988).
- [46] F. H. Mies, C. J. Williams, P. S. Julienne, and M. Krauss, *J. Res. Natl. Inst. Stand. Technol.* **101**, 521 (1996).
- [47] V. Kokoouline, O. Dulieu, R. Kosloff, and F. Masnou-Seeuws, *J. Chem. Phys.* **110**, 9865 (1999).
- [48] K. Willner, O. Dulieu, and F. Masnou-Seeuws, *J. Chem. Phys.* **120**, 548 (2004).
- [49] S. Kallush and R. Kosloff, *Chem. Phys. Lett.* **433**, 221 (2006).
- [50] B. Zygelman and A. Dalgarno, *Phys. Rev. A* **38**, 1877 (1988).
- [51] P. S. Julienne, *J. Chem. Phys.* **68**, 32 (1978).
- [52] J. Tellinghuisen and P. S. Julienne, *J. Chem. Phys.* **81**, 5779 (1984).
- [53] O. P. Makarov, R. Côté, H. Michels, and W. W. Smith, *Phys. Rev. A* **67**, 042705 (2003).
- [54] R. Côté and A. Dalgarno, *Phys. Rev. A* **62**, 012709 (2000).
- [55] B. R. Johnson, *J. Chem. Phys.* **69**, 4678 (1978).
- [56] K. Sando and A. Dalgarno, *Mol. Phys.* **20**, 103 (1971).
- [57] R. Napolitano, J. Weiner, C. J. Williams, and P. S. Julienne, *Phys. Rev. Lett.* **73**, 1352 (1994).
- [58] NIST Atomic Spectra Database <http://physics.nist.gov/PhysRefData/ASD>.
- [59] R. W. Molof, H. L. Schwartz, T. M. Miller, and B. Bederson, *Phys. Rev. A* **10**, 1131 (1974).
- [60] W. E. Cooke, T. F. Gallagher, R. M. Hill, and S. A. Edelstein, *Phys. Rev. A* **16**, 1141 (1977).
- [61] V. A. Dzuba and A. Derevianko, *J. Phys. B: At. Mol. Opt. Phys.* **43**, 074011 (2010).
- [62] M. Tomza, W. Skomorowski, M. Musial, R. Gonzalez Ferez, C. P. Koch, and R. Moszynski, *Mol. Phys.* **111**, 1781 (2013).
- [63] H. Da Silva, Jr., M. Raoult, M. Aymar, and O. Dulieu, [arXiv:1501.06385v2](https://arxiv.org/abs/1501.06385v2).
- [64] T. G. A. Heijmen, R. Moszynski, P. E. S. Wormer, and A. van der Avoird, *Mol. Phys.* **89**, 81 (1996).
- [65] Z. Idziaszek, A. Simoni, T. Calarco, and P. S. Julienne, *New J. Phys.* **13**, 083005 (2011).
- [66] Z. Idziaszek, T. Calarco, P. S. Julienne, and A. Simoni, *Phys. Rev. A* **79**, 010702 (2009).
- [67] E. R. Sayfutyarova, A. A. Buchachenko, S. A. Yakovleva, and A. K. Belyaev, *Phys. Rev. A* **87**, 052717 (2013).
- [68] P. Pellegrini, M. Gacesa, and R. Côté, *Phys. Rev. Lett.* **101**, 053201 (2008).
- [69] P. S. Żuchowski and J. M. Hutson, *Phys. Rev. A* **79**, 062708 (2009).
- [70] S. Ghosal, R. J. Doyle, C. P. Koch, and J. M. Hutson, *New J. Phys.* **11**, 055011 (2009).
- [71] W. Skomorowski, M. L. Gonzalez-Martinez, R. Moszynski, and J. M. Hutson, *Phys. Chem. Chem. Phys.* **13**, 19077 (2011).
- [72] T. G. Heijmen, R. Moszynski, P. E. Wormer, A. van der Avoird, A. D. Rudert, J. B. Halpern, J. Martin, W. B. Gao, and H. Zacharias, *J. Chem. Phys.* **111**, 2519 (1999).
- [73] K. M. Jones, E. Tiesinga, P. D. Lett, and P. S. Julienne, *Rev. Mod. Phys.* **78**, 483 (2006).
- [74] C. Chin, R. Grimm, P. S. Julienne, and E. Tiesinga, *Rev. Mod. Phys.* **82**, 1225 (2010).
- [75] A. Simoni and J.-M. Launay, *J. Phys. B: At. Mol. Opt. Phys.* **44**, 235201 (2011).
- [76] J. M. Hutson, M. Beyene, and M. L. González-Martinez, *Phys. Rev. Lett.* **103**, 163201 (2009).